Dalton Transactions

ROYAL SOCIETY OF CHEMISTRY

PAPER

View Article Online
View Journal | View Issue

Cite this: *Dalton Trans.*, 2024, **53**, 19351

Oxaphosphiranes: isolable phosphorus-containing epoxide rings†

Niklas Volk,‡[a] Antonio García Alcaraz,‡[b] Selvakumar Balasubramaniam,[a] Jannik Heumann,[a] Gregor Schnakenburg,[a] Arturo Espinosa Ferao *[b] and Rainer Streubel *[a]

Received 18th October 2024,
Accepted 22nd October 2024

DOI: 10.1039/d4dt02915a

rsc.li/dalton

Combining different heteroatoms in an epoxide-type ring having Lewis basic and acidic characteristics is challenging as it creates an increasing number of polar bonds and high ring strain energy. The first examples of isolable oxaphosphiranes, *i.e.*, epoxide rings with a phosphorus atom, have been synthesized using a facile and effective protocol starting from [pentacarbonyl{dichloro(trityl)phosphane}molybdenum (0)] (trityl = CPh_3), *tert*-butyllithium and commercially available fluorinated benzaldehydes. Reactions with various acids and bases will be described. Theoretical results unveil a singlet carbene-like FMO situation at phosphorus in oxaphosphirane, which is used to explain reaction mechanisms.

Introduction

Epoxides[1] (**I**) (Fig. 1), cyclopropanes containing one oxygen instead of a carbon atom in the ring, are versatile reagents,[2] and their oxidation can serve as a protecting strategy for alkenes. For example, due to their polar C–O bonds and high ring strain energy (RSE), ring opening reactions can be initiated easily, which makes them highly potent monomers in polymer synthesis.[3] Owing to the rich chemistry of epoxides, investigating heavier analogues and those possessing a second ring heteroatom has been a subject of great interest. Although small inorganic ring systems have been intensively explored,[4] examples of heavy analogues of epoxides are still scarce. It is known that the presence of an additional heteroatom in the ring has a significant influence on its stability and reactivity. This is illustrated by a series of main group element-containing epoxides of groups 14–16 also starting with structurally confirmed oxasiliranes (**II**). The latter were exclusively accessed through the reaction of a bulky dialkylsilylene with a ketone,[5] but their chemistry is almost unknown.

The latter might be due to the high RSE value (estimated through the additive method based on bond contributions as 33.61 (ref. 6) and 34.22 (ref. 7) kcal mol^{-1}; accurately computed through homodesmotic reactions as 38.70 (ref. 6) kcal mol^{-1}). In contrast, oxaziridines (**III**) are easily accessed and, hence, well established in organic synthetic chemistry.[8] For example, oxidizing imines using peroxy acids is one of the common methods to prepare derivatives of **III**.[8] Dioxiranes (**V**) are also available, *e.g.*, as dimesityl derivatives synthesized by photooxidation of an *in situ* generated carbene in air, as reported by Sander, but the compound is stable only below −20 °C.[9] Again, including a third row element from group 16 diminishes the thermal stability and, hence, oxathiirane (**VI**) is known only in argon matrices at low temperature.[10]

The search for phosphorus homologues of oxaziridines, *i.e.*, oxaphosphiranes (**IV**), started with metal complexes such as **VII**, reported by Mathey *et al.* in 1990,[11] relying on the oxidation of *end*-on phosphaalkene pentacarbonyltungsten(0) complexes. Despite being a synthetic breakthrough, the multistep protocol was too tedious to allow for broader studies. Even the subsequent new protocol, reported by Streubel[12] – the trapping of an *in situ* generated terminal phosphinidene

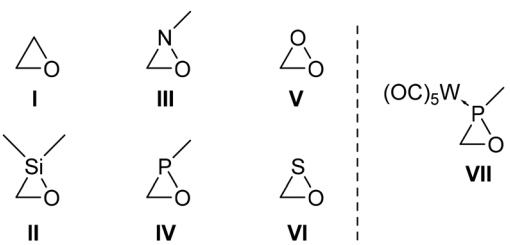

Fig. 1 Epoxide (**I**) and heteroatom-containing analogues (**II**–**VI**); lines denote ubiquitous substituents.

[a]*Institut für Anorganische Chemie, der Rheinischen Friedrich-Wilhelms-Universität Bonn, Gerhard-Domagk-Str. 1, 53121 Bonn, Germany. E-mail: r.streubel@uni-bonn.de*
[b]*Departamento de Química Orgánica, Facultad de Química, Universidad de Murcia, Campus de Espinardo, 30100 Murcia, Spain. E-mail: artuesp@um.es*

†Electronic supplementary information (ESI) available: Experimental protocols, NMR spectra, X-ray data and computational results. CCDC 2382051–2382055. For ESI and crystallographic data in CIF or other electronic format see DOI: https://doi.org/10.1039/d4dt02915a

‡These authors contributed equally to this work.

complex – turned out to be only a slight improvement. The real breakthrough came in 2007 when we significantly improved the methodology[13] by using Li/Cl phosphinidenoid complexes and a great variety of aldehydes and ketones, even bearing other functional groups.[14] In the following decade, numerous transformations became accessible, thus illustrating the great synthetic potential of the oxaphosphirane ring system.[15]

However, the masking of the phosphorus lone pair *via* coordination to a transition metal center precluded the exploration of the chemistry of unligated derivatives. The search for unligated oxaphosphiranes **VI** started with Ramirez in 1968, when hexafluoroacetone reacted with phosphanes to yield dioxaphospholanes.[16] Later, the pathway was investigated theoretically, thus showing that intermediate $\sigma^5\lambda^5$-oxaphosphiranes are likely to be involved.[17] In 1993, Röschenthaler *et al.* reported the [2 + 1]-cycloaddition of an iminophosphane to hexafluoroacetone, thus forming a σ^4,λ^5-oxaphosphirane; it should be noted that no structural confirmation was provided.[18] Very recently, we demonstrated that 1,3-di-*tert*-butyloxaphosphirane can be obtained from a pentacarbonylmolybdenum(0) complex *via* a thermal reaction with diphenylphosphinoethane (DPPE).[19] The product was obtained exclusively as toluene solution, thus precluding various interesting investigations, and no X-ray structure could be obtained. Therefore, we restarted the search for a novel method to access isolable, unligated oxaphosphiranes that would allow for broad investigations. Furthermore, we hypothesized that the ring carbon atom should possess fluorine-containing substituents, based on the conclusions of a theoretical study.[20]

Herein, we describe a new facile protocol for oxaphosphirane liberation from metal(0) complexes using *N*-methylimidazole under thermal conditions. Its molecular solid-state structure is discussed and the bonding was analysed using high-level theoretical investigations. Reactions of the isolated oxaphosphiranes with various reagents such as water (H_2O and D_2O), tetrachloro-*ortho*-benzoquinone (TOB), an acid (HCl) and a base/nucleophile (an N-heterocyclic carbene) are reported.

Results and discussion

Oxaphosphirane molybdenum complexes **3a** and **3b** and the oxaphosphirane tungsten complex **3c** were prepared according to our protocol[14b,21] *via in situ* formed Li/Cl phosphinidenoid complex **2**[22] using fluorinated benzaldehyde derivatives, resulting in moderate yields (50–65%) (Scheme 1).

The molecular structures of **3b** and **3c** were confirmed by single crystal X-ray diffraction studies (Fig. 2). In comparison with known oxaphosphirane molybdenum[23] and tungsten[21] complexes with fluorinated aryl C-substituents, the most important differences can be observed in slightly elongated P–M bonds (P–Mo: 2.4872(14) Å (**3b**) *vs.* 2.467(2) Å;[23] P–W: 2.4715 (13) Å (**3c**) *vs.* 2.4630(11) Å (ref. 21)).

Following previous investigations on ligand decomplexation from molybdenum complexes using DPPE as a chelating ligand under thermal conditions,[19] which were successful for

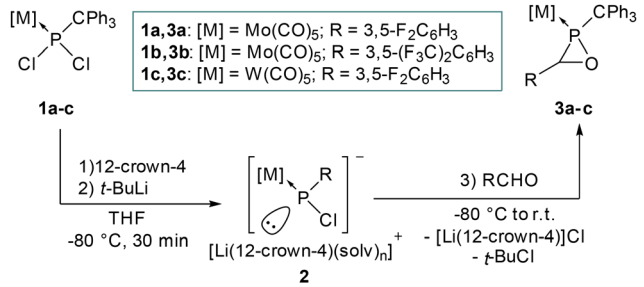

Scheme 1 Synthesis of [Mo] (**3a** and **b**) and [W] oxaphosphirane (**3c**) complexes.

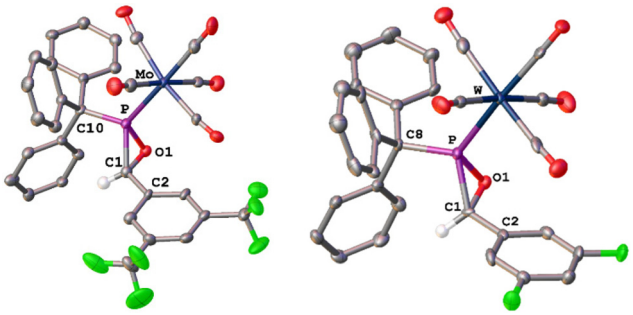

Fig. 2 Single crystal structures of **3b** and **3c** (50% probability) The hydrogen atoms, except the ones at the ring carbons, are omitted for clarity. **3b**: selected bond lengths/Å: P–Mo 2.4872(14), P–O1 1.673(4), P–C1 1.802(5), and O1–C1 1.458(6); selected bond angles/°: O1–P–C1 49.5(2), P–C1–O1 60.7(2), and P–O1–C1 69.9(2); **3c**: selected bond lengths/Å: P–W 2.4715(13), P–O1 1.669(4), P–C1 1.790(5), and O1–C1 1.481(7); selected bond angles/°: O1–P–C1 50.5(2), P–C1–O1 60.5(3), and P–O1–C1 69.6(3).

the *P*-*t*-Bu substituted oxaphosphirane ligand, we achieved the decomplexation of the oxaphosphirane ligands in **3a** and **b**. Unfortunately, here an inseparable mixture of the oxaphosphiranes and non-identified by-products was obtained.

Therefore, an alternative protocol needed to be developed. Inspired by the decomplexation of 1*H*-phosphirenes using sequentially elemental iodine and 1-methylimidazole, described by Mathey,[24] we decided to examine this for **3a** and **3b**. Heating solutions only with 4 eq. of 1-methylimidazole resulted in a clean liberation of the oxaphosphiranes **4a** and **4b** (Scheme 2), having almost identical ^{31}P-NMR resonances (−26.0 (**4a**) and −25.5 ppm (**4b**)).

Compounds **4a** and **4b** were fully characterized by NMR, mass spectrometry, IR and elemental analysis. Additional column chromatography (Al_2O_3/ether) at low temperature (0 to −10 °C) can be used for purification, but this results in diminished yields (loss: 15–20%). Suitable single crystals for X-ray diffraction measurements of **4b** were obtained (Fig. 3), confirming the molecular structure of an unligated oxaphosphirane having the *trans*-conformation as in the precursor. The molecular structure of **4b** contained only the 2*S*,3*R*-enantiomer with the two substituents at P and C in the *trans*-position as identified by the Flack parameter[25] of 0.00(18). In comparison

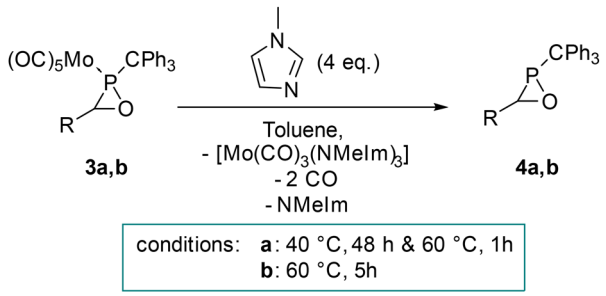

Scheme 2 Decomplexation of the oxaphosphirane ligands **4a** and **b**.

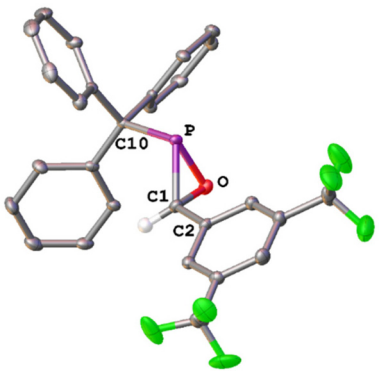

Fig. 3 Single crystal molecular structure of **4b** (50% probability). The hydrogen atoms, except the one at the ring carbon, are omitted for clarity. Selected bond lengths/Å: P–O1 1.682(3), P–C1 1.819(4), and O1–C1 1.458(5); selected bond angles can be found in Table 1.

with the crystal structure of **3b**, only very small differences could be identified, *i.e.*, smaller O1–P–C10 and P–C1 C2 angles (Table 1).

It is worth highlighting that the original protocol of Mathey[24] was not successful in our study.

Pentacoordinate oxaphosphiranes have been previously reported[26] and, most often, assumed to be short-lived intermediates. Recently, we obtained first, albeit weak, evidence in the reaction of the *P*-*t*-Bu substituted oxaphosphirane with TOB *via* VT-$^{31}P\{^1H\}$ NMR spectroscopy at low temperature, but the characterization remained incomplete. As pentacoordinate phosphirenes have been accessed *via* a reaction with TOB,[27] we decided to investigate the reaction of **4a** with TOB in CH_2Cl_2 (Scheme 3).

Table 1 Selected bond angles of **4b** and **3b**

Bond angles/°	4b	3b
O1–P–C1	49.04(16)	49.5(2)
P–C1–O1°	60.57(19)	60.7(2)
P–O1–C1	70.4(2)	69.9(2)
P–C1 C2	118.0(3)	124.5(4)
C1–P C10	110.74(18)	105.3(2)
O1–P–C10	104.99(16)	108.9(2)

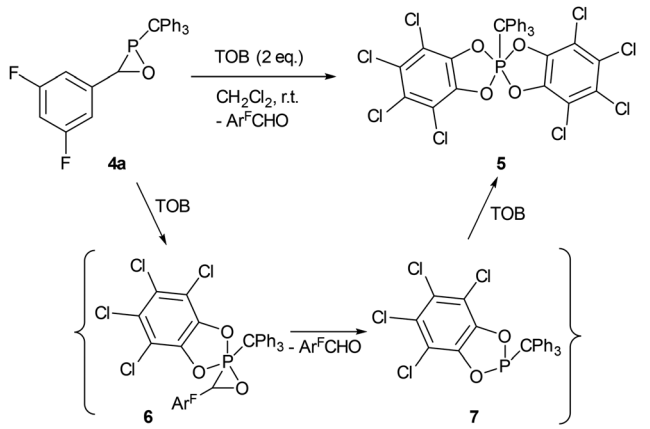

Scheme 3 Synthesis of the spirobisbenzodioxaphosphole **5** and the proposed reaction mechanism involving $\sigma^5\lambda^5$-oxaphosphirane **6** and $\sigma^3\lambda^3$-benzodioxaphospholane **7**.

First, the reaction with 1 eq. of TOB was carried out at room temperature, and after 2 h, a 1 : 1 mixture of **4a** showed product **5** at 1.7 ppm in the $^{31}P\{^1H\}$-NMR spectrum. By subsequently adding 1 eq., a full conversion to **5** was observed. Mass spectrometry showed the isotopic pattern of the molecular ion peak (*m*/*z* 765.8 $[M]^{\bullet+}$ (EI)), indicating a structural motif with eight chlorine atoms, and the exact mass corresponded to the known *P*-CPh_3 substituted spirobisbenzodioxaphosphole.[28] VT-$^{31}P\{^1H\}$ NMR studies from −70 °C to r.t. did not reveal an intense signal that could be safely assigned to the intermediately formed pentacoordinate oxaphosphirane **6**. However, at −10 °C, a signal with very low intensity at 208.2 ppm can be assigned to the *P*-CPh_3 substituted dioxaphospholene **7**[28] (δ $^{31}P\{^1H\}$ = 208.5 ppm). The formation of **7** provided further insight into the reaction mechanism, pointing to a preceding formation of the $\sigma^5\lambda^5$-oxaphosphirane **8**, followed by a loss of the aldehyde. This is followed by the addition of a second TOB unit to yield the final product **5**. To gain a deeper understanding of the reaction mechanism, theoretical studies were performed (*vide infra*).

Quantum chemical (QC) calculations ($CPCM_{toluene}$/PWPB95-D3/def2-QZVPP//$CPCM_{toluene}$/PBEh-3c) were performed using the model compound **4a′**, where the *P*-CPh_3 (trityl) substituent was replaced by *t*-Bu. The two individual steps of the reaction with TOB are very exergonic ($\Delta\Delta G \approx -46$ kcal mol^{-1}) and proceed over a rather low barrier ($\Delta\Delta G^{\ddagger} \approx 19$ kcal mol^{-1}), whereas the loss of the aldehyde unit is moderately exergonic with a slightly higher barrier (Fig. 4).

In our recent report on the *P*-*t*-Bu substituted oxaphosphirane,[19] obtained as solution only, we observed great moisture sensitivity; the latter is in stark contrast to the case of oxaphosphirane complexes. This abovementioned unusual sensitivity of the free oxaphosphirane prompted us to investigate the reactivity of **4a** towards water. Oxaphosphirane **4a** was dissolved in THF-d_8 and small amounts of water were added (Scheme 4).

At ambient temperature, no reaction was observed, and after heating to 40 °C, a rather slow conversion to three pro-

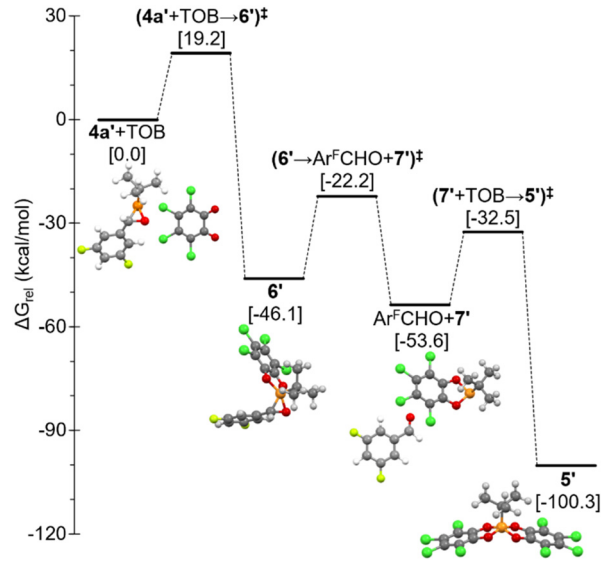

Fig. 4 Computed ($CPCM_{toluene}$/PWPB95-D3/def2-QZVPP//$CPCM_{toluene}$/PBEh-3c) Gibbs energy profile for the oxidation of model **4a′** with TOB.

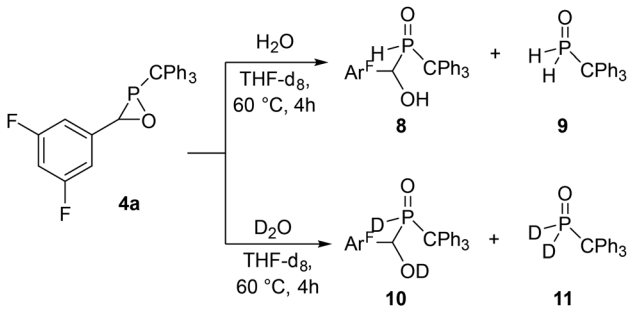

Scheme 4 Investigations of the reactivity of **4a** towards H_2O (or D_2O), resulting in the formation of diastereomers **8** (or **10**) and the primary phosphane oxide **9** (or **11**).

ducts, two diastereomers (*vide infra*) of secondary phosphane oxide **8** (δ $^{31}P\{^1H\}$ = 50.3 and 49.3 ppm) and the *P*-CPh_3 substituted phosphane oxide **9** (δ $^{31}P\{^1H\}$ = 19.9 ppm), were observed; at 60 °C, the reaction was complete in 4 h. The product mixture was investigated by NMR and IR spectroscopy, and the molecular structure of **8** was confirmed by an X-ray diffraction study. The elemental cell contained both diastereomers and two molecules of CH_2Cl_2. The crystal structure revealed intra- and intermolecular interactions between a total of three formula units of **8** and the solvent, as depicted in Fig. S39 (ESI†). The bond lengths and bond angles are in accordance with those of a literature known *P*-Mes substituted secondary phosphane oxide.[29] To gain further insight into the origin of the hydrogen atoms on the phosphorus center, the reaction was repeated with D_2O (Scheme 4). This resulted in the formation of the deuterated phosphane oxide diastereomers **10** (δ $^{31}P\{^1H\}$ = 50.2 ppm, t*, $^1J_{P,D}$ = 73.7 Hz; 49.5 ppm, t*, $^1J_{P,D}$ = 74.0 Hz) and **11** (δ $^{31}P\{^1H\}$ = 19.5 ppm, quint*, $^1J_{P,D}$ = 74.4 Hz), proving the origin of the hydrogen atoms from the reagent water. The molecular structure of **10** was also confirmed by X-ray crystallography (Fig. 5), and the structure revealed, in contrast to the molecular structure of **8**, the formation of a bridging dimer between the PO and the OD groups. The distance between the oxygen atoms of the PO group and the OD group of another formula unit (d(O1···O2) = 2.709 Å) is in good accordance with the bridging dimer of a literature known tertiary phosphane oxide[30] (d(O1···O2) = 2.682(3) Å).

Quantum chemical calculations at the working level of theory (THF was employed for the continuum solvation model) using the same simplified compound **4a′** revealed that initial ring opening can proceed through a nucleophilic attack on either the C or P ring atoms, in agreement with the reported behaviour for P-complexed oxaphosphiranes.[14c] Similar to the previous report, the attack by two, three and five explicit water molecules was explored. The approach of only one H_2O molecule was not inspected, as the very similar methanolysis reaction of the parent oxaphosphirane with one MeOH molecule was reported to occur over a rather high-lying transition state.[31] In the case of two H_2O molecules (see Fig. S51†), only ring opening by attack on C was observed, leading to zwitterion *l*-**12**, which then readily undergoes an internal acid–base reaction (most likely occurring intermolecularly through a chain of water molecules) to yield the stable phosphinic acid **13** (Scheme 5). When there is excess water, the energy barrier of this ring opening ($\Delta\Delta G^{\ddagger}$ = 31.0 kcal mol^{-1}) can be considered as the energy difference between the TS (transition state) and the initial van der Waals complex **4a′**·2H_2O. As the starting oxaphosphirane is racemic, the 2*R*,3*S* (unlike or '*u*') configuration was chosen, in agreement with the

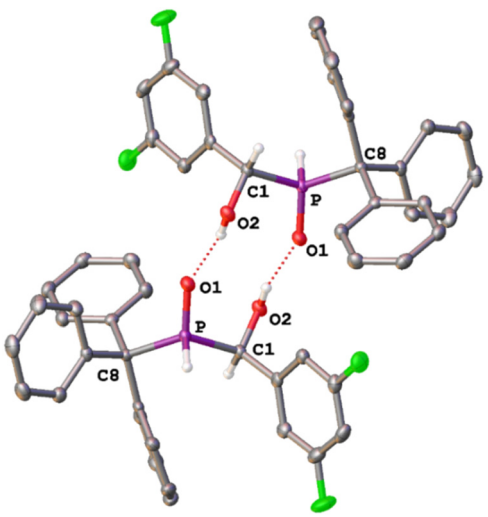

Fig. 5 D-bridging dimer of the molecular structure of **10** (enantiomers 1*R*,2*S* and 1*S*,2*R*) with co-crystallized CH_2Cl_2 in the single crystal (50% probability level). Hydrogen atoms, except deuterium ones and the hydrogen atom at C1, are omitted for clarity. Selected bond lengths/Å: O1–O2 2.709, P–O1 1.4895(12), P–C1 1.8774(18), and P–C8 1.8746(17); selected bond angles/°: O1–P–C1 111.08(7) and 116.34(7).

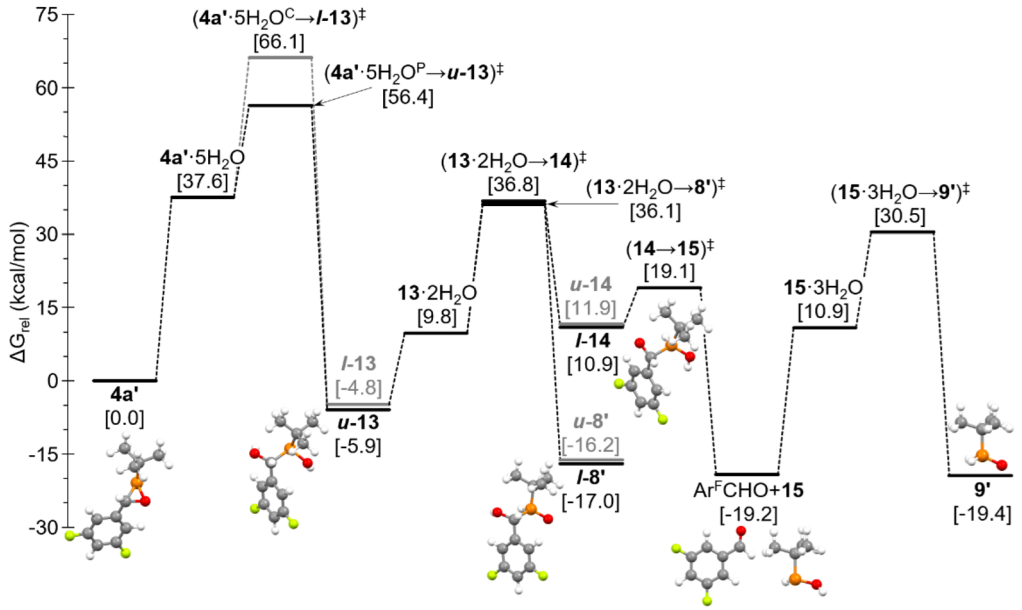

Fig. 6 Computed ($CPCM_{THF}$/PWPB95-D3/def2-QZVPP//$CPCM_{THF}$/PBEh-3c) Gibbs energy profile for the hydrolysis of model **4a′**.

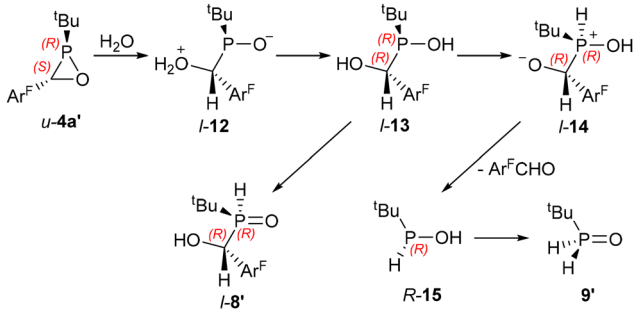

Scheme 5 Proposed mechanism for the reaction of model **4a′** with H_2O. Stereochemistry corresponds to the C-attack of H_2O. All species except **9′** are racemates.

observed *trans*-arrangement observed in the single crystal molecular structure of **4b**. Ring opening proceeds with inversion only at the C atom, thus resulting in an *l*-**13** diastereomeric pair. The use of three H_2O molecules (see Fig. S51†) favors attack on P, affording the other most stable diastereomeric pair *u*-**13** ($\Delta\Delta G_{l/u}$ = 1.1 kcal mol^{-1}) with no inversion at either P or C (*i.e.*, the diastereomer of that depicted in Scheme 5) and over a lower barrier ($\Delta\Delta G^{\ddagger}$ = 27.0 kcal mol^{-1}). When a chain of five H_2O molecules is included, even lower energy barriers are obtained, with preferential P ($\Delta\Delta G^{\ddagger}$ = 18.8 kcal mol^{-1}) over C attack ($\Delta\Delta G^{\ddagger}$ = 28.5 kcal mol^{-1}) (Fig. 6), forming *u*-**13** and *l*-**13**, respectively. Despite the significantly most favored P-attack in model *u*-**4a′**, the larger steric demand of the P-trityl group in **4a** should favor C-attack to some extent. The resulting *l*-**13** intermediate was thus used to describe the rest of the mechanistic sequence (Scheme 5 and Fig. 6).

The slightly exergonic isomerization of the phosphinic acid moiety [>P–OH] in *l*-**13** to the more stable P-oxide [>P(H)═O] group results in the final (model) product *l*-**8′**, through a rather high barrier ($\Delta\Delta G^{\ddagger}$ = 50.5 kcal mol^{-1}) O-to-P [1,2]H shift (see Fig. 6). When this O-to-P hydrogen atom transfer occurs with the assistance of one or two water molecules, the energy barrier decreases significantly ($\Delta\Delta G^{\ddagger}$ = 28.5 and 26.3 kcal mol^{-1}, respectively) (Fig. 6). Similarly, starting from *u*-**13**, the slightly less stable P-oxide product *u*-**8′** ($\Delta\Delta G_{l/u}$ = 0.9 kcal mol^{-1}) is obtained (the energy profile for this diastereomeric transformation is not shown). The occurrence of two diastereomers of the real *P*-CPh_3 substituted species **8**, as shown in the NMR spectra, is due to the occurrence of competitive C- and P-attack hydrolysis pathways, leading to *l*- and *u*-**8**, respectively.

The intermediate *l*-**13** undergoes transprotonation to yield another more stable betaine *l*-**14** that very readily experiences C–C bond cleavage, furnishing 3,5-difluorobenzaldehyde (Ar^FCHO) and *tert*-butyl phosphinic acid (*R*-**15**). Interestingly, the latter can be formally considered as a product resulting from the addition of H_2O to a phosphinidene unit; the latter is not formed during hydrolysis, but is present/masked in the oxaphosphirane **4a′**. This compound **15** isomerizes to the most stable phosphane oxide **9′**, either intramolecularly, with a rather high TS ($\Delta\Delta G^{\ddagger}$ = 61.3 kcal mol^{-1}), or through one ($\Delta\Delta G^{\ddagger}$ = 29.8 kcal mol^{-1}), two ($\Delta\Delta G^{\ddagger}$ = 30.8 kcal mol^{-1}) (see Fig. 6) or three ($\Delta\Delta G^{\ddagger}$ = 19.6 kcal mol^{-1}) water molecules (Fig. 6). The same outcome results from starting with diastereomeric *u*-**13** *via* the slightly less stable betaine *u*-**14** ($\Delta\Delta G_{l/u}$ = 1.0 kcal mol^{-1}) (energy profile not shown).

The theory-based indication of a nucleophilic attack of the oxygen atom of water prompted us to study the reactivity towards other ambident reagents. Thus, the reaction of oxaphosphirane **4a** with hydrochloric acid in diethyl ether was investigated.[14a,c,32] In contrast to the expected formation of an acyclic product stemming from cleavage of the P–O bond,

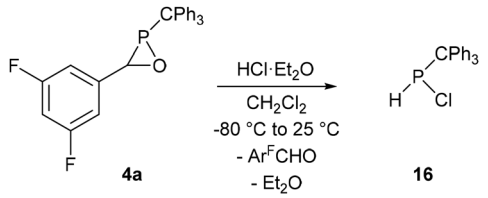

Scheme 6 Synthesis of the *P*-CPh_3 chlorophosphane **16**.

which was observed before for other oxaphosphirane complexes, the (complete) ring cleavage product **16** was obtained (Scheme 6); this product had been obtained earlier by Plack using a classical reduction route.[33]

The ^{31}P-NMR spectrum displayed a doublet with a chemical shift of 44.9 ppm and a coupling constant of $^{1}J_{P,H}$ = 189.9 Hz. The signal shoulder (ratio 1 : 3) supports the directly bound chlorine atom to phosphorus, *i.e.*, showing the overlap of the two signals of the two P–Cl isotopomers.

The calculated energy profile for the model reaction of **4a′** (Fig. 7) shows that the first step is the slightly exergonic 1,1-addition of HCl to the P-center, thus exhibiting singlet phosphinidene-like reactivity, furnishing the $\sigma^5\lambda^5$-oxaphosphirane intermediate **17**. This species displays a proper trigonal bipyramidal arrangement at P with elongated axial P–O (d = 1.740 Å, MBO 0.795) and P–Cl (d = 2.243 Å, MBO 0.685) bonds (O–P–Cl angle – 153.0°). Driven by the relief of ring strain energy, this intermediate undergoes a low barrier exergonic chelotropic [2 + 1]-cycloreversion, leading to the final (model) chlorophosphane **16′** *via* the loss of the aldehyde unit (Fig. 7).

Since the reaction of the oxaphosphirane **4a** with the strong acid led to the elimination of the aldehyde unit, its reactivity towards a nucleophile – being also basic at the same time – was explored, hoping to obtain a ring-opened zwitterionic product. When 1,3,4,5-tetramethyl-imidazol-2-ylidene (IMe_4) was allowed to react with the title compound, the aldehyde was eliminated, again. To obtain a more robust product having a greater tendency to crystallize, the primarily formed IMe_4-P-CPh_3 **18** was treated with $W(CO)_5$(NCMe) and yielded $W(CO)_5$ complex **19** (Scheme 7), which was known before. A ^{31}P-NMR signal was observed at −37.7 ppm with a $^{1}J_{P-W}$ coupling constant magnitude of 114.08 Hz. The molecular structure of compound **19** in the solid state (Fig. 8) shows the (typical) geometrical features of a (zwitterionic) IMe_4-stabilized phosphinidene complex.

The (theoretical) energy profile for this reaction was obtained using the very simplified model **4a″** featuring a methyl substituent at P and 1,3-dimethylimidazol-2-ylidene (here designated as NHC^{Me_2}) (Fig. 9). The initially formed encounter complex **4a″**·NHC undergoes almost barrierless exergonic chelotropic cycloreversion with the loss of the aldehyde unit and affording the corresponding (model) phosphinidene-NHC adduct **18″**.

The formation of the encounter complex can be understood in terms of pnictogen bonding, where the approaching nucleophile donates electron density into the "σ-hole", which conceptually corresponds to the σ*(P–O) orbital. This is visualized by the LUMO having antibonding characteristics for both the P–C and the P–O endocyclic bonds (Fig. 10a). The corresponding bonding interaction between the P and the CO fragments corresponds to the HOMO, thus pointing to singlet phosphini-

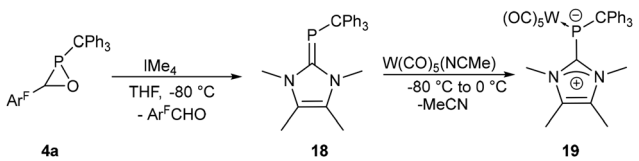

Scheme 7 Reaction of **4a** with IMe_4 and $W(CO)_5$(NCMe).

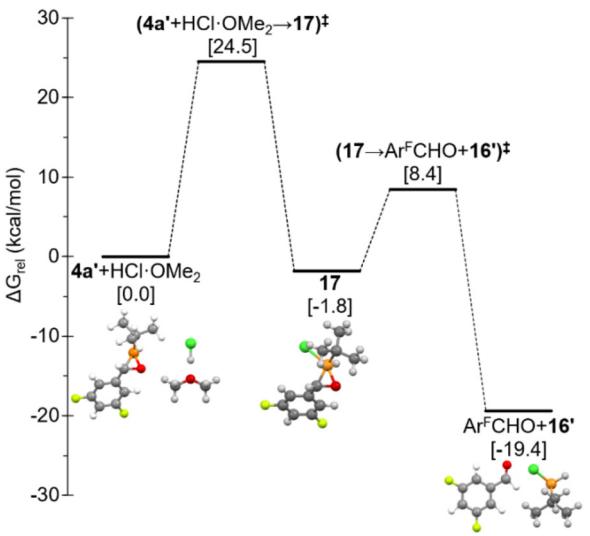

Fig. 7 Computed ($CPCM_{CH_2Cl_2}$/PWPB95-D3/def2-QZVPP//$CPCM_{CH_2Cl_2}$/PBEh-3c) Gibbs energy profile for the reaction of model **4a′** with HCl using Me_2O as a model for Et_2O.

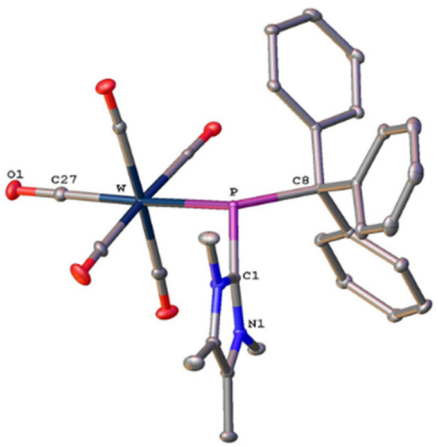

Fig. 8 Solid state structure of compound **19** (50% probability level). Hydrogen atoms are omitted for clarity. Selected bond lengths/Å: C8–P 1.955(17), C1–P 1.850(18), P–W 2.615(5), W–C27 1.983(2), and C27–O1 1.154(3); selected bond angles/°: W–P–C8 122.37(5), W–P–C1 108.98 (6), and C1–P–C8 106.50(8).

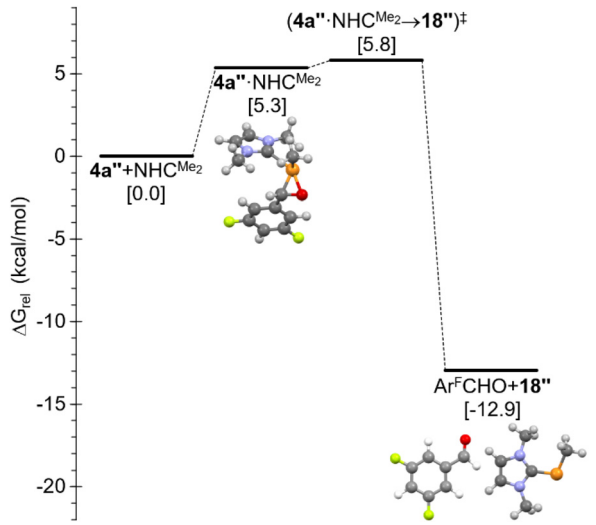

Fig. 9 Computed (CPCM$_{toluene}$/PWPB95-D3/def2-QZVPP//CPCM$_{toluene}$/PBEh-3c) Gibbs energy profile for the reaction of model **4a''** with NHC^{Me_2}.

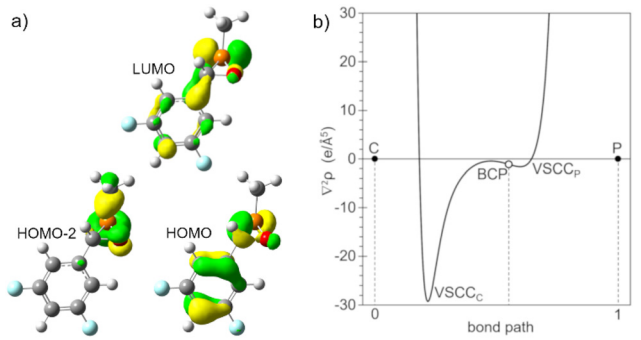

Fig. 10 (a) Computed [CPCM$_{toluene}$/PWPB95-D3/def2-QZVPP//CPCM$_{toluene}$/PBEh-3c] Kohn–Sham frontier molecular orbital isosurfaces (0.06 – isovalue) for oxaphosphirane **4a''**. (b) Variation of the Laplacian of electron density along the pnictogen C···P bond path for the ionic-enhanced dative bonding in **4a''**·NHC.

dene characteristics of the R–P fragment, which locates the P lone pair at HOMO−2. By populating the LUMO, the P–C and P–O bonds are weakened, facilitating the detachment of the aldehyde. Therefore, the removal of the carbonyl fragment from oxaphosphiranes upon nucleophilic attack on phosphorus could be potentially used as an important synthetic technique to introduce the *P*-CPh$_3$ moiety into a targeted nucleophilic substrate. It is interesting to highlight the resemblance of these FMOs exhibited by the PR fragment in a $\sigma^3\lambda^3$-oxaphosphirane to those of singlet carbene-type features, showing filled (HOMO–2 in **4a''**) and vacant (HOMO and LUMO in **4a''**) p-type atomic orbitals (Fig. 10a).

The nature of the NHC–P bond in **4a''**·NHC was analyzed following a well-established protocol[34] based on the analysis of the Laplacian of the electron density along the central part of the NHC–P bond path. In the case of **4a''**·NHC, a rather short P···C distance (d = 2.130 Å) is observed and the plot along the P···C bond path exhibits a small negative value of the Laplacian at the BCP ($\nabla^2\rho$ = −1.098 e Å^{-5}) with the two VSCC (valence-shell charge concentration) bands located at the two different basins (each side of the BCP) with a small negative relative charge concentration band position parameter, τ_{VSCC} = −0.016 (Fig. 10b). These features correspond to ionic-enhanced dative bonding, according to a very recent description.[35]

Conclusions

Herein, a new synthetic protocol to obtain stable and isolable oxaphosphiranes is described using a combination of kinetic protection of the P-center and the ring bond(s) strengthening effect of fluorinated C-bound aryl groups. These first isolated unligated oxaphosphiranes were obtained *via* decomplexation from molybdenum(0) complexes using (cheap) *N*-methyl-imidazole under thermal conditions; the newly formed complex [Mo(CO)$_3$(NMeIm)$_3$] can be easily separated and, hence, offer the option to be recycled. Reactivity studies on such oxaphosphiranes were performed using one derivative as a case in point. The reaction with tetrachloro-*ortho*-benzoquinone (TOB) led to oxidation of phosphorus and elimination of the aldehyde unit, finally. A similar reaction outcome was observed in reactions with acidic reagents (H$_2$O and HCl) as well as with a nucleophilic and basic reagent such as IMe$_4$, both leading to ring cleavage and the elimination of the aldehyde unit.

Computational analysis shows that full oxidation with TOB takes place in three exergonic low-barrier steps. The hydrolysis proceeds by preferential P- over C-attack of water on the ring in model compounds with only moderate steric bulk at phosphorus, although it could be expected to be reversed in *P*-trityl substituted derivatives. The initially formed phosphinic acid rearranges to yield the final phosphane oxide. However, it can also eliminate an aldehyde unit, affording a new phosphinic acid as a precursor of a primary phosphane oxide R-PH$_2$(O). A reaction with HCl or an NHC derivative furnishes P-addition products as a result of the remarkable reactivity feature of a formal singlet phosphinidene being (still) part of the oxaphosphirane. To the best of our knowledge, the latter bonding feature of a $\sigma^3\lambda^3$-P center in a heterocycle is of particular importance, which has not been reported for small rings, so far. It should also be noted that geometrically distorted, T-shaped cyclic phosphanes show a similar reactivity.

Author contributions

Conceptualization: R. S. and A. E. F.; methodology: N. V., S. B. and A. G. A.; validation: A. E. F. and R. S.; formal analysis and investigation: N. V., J. H., S. B. and A. G. A.; resources: R. S. and A. E. F.; data curation: A. E. F. and R. S.; writing—review and editing: A. E. F. and R. S.; and supervision: A. E. F. and R. S. All authors have read and agreed to the published version of the manuscript.

Data availability

Electronic supplementary information available: experimental protocols, NMR spectra, X-ray diffraction data and theoretical results.

Conflicts of interest

There are no conflicts to declare.

Acknowledgements

This work was conducted in memory of Prof. Dr E. Niecke and Prof. Dr F. Mathey and to honor their ground-breaking discoveries in the chemistry of small P-heterocycles.

The authors are grateful to the Deutsche Forschungsgemeinschaft (STR 411/29-3), the University of Bonn, for financial support (R. S.), to the Servicio de Cálculo Científico at the University of Murcia for technical support and computational resources (A. E. F. and A. G. A.), and to the University of Murcia for a pre-doctoral fellowship (A. G. A).

References

1 (*a*) A. Wurtz, *Liebigs Ann. Chem.*, 1859, **110**, 125; (*b*) S. Rebsdat and D. Mayer, in *Ullmann's encyclopedia of industrial chemistry*, Wiley-VCH, Wiley online library, Weinheim, 7th edn, 2010.
2 R. E. Parker and N. S. Isaacs, *Chem. Rev.*, 1959, **59**, 737.
3 H. Q. Pham and M. J. Marks, in *Ullmann's encyclopedia of industrial chemistry*, Wiley-VCH, Wiley online library, Weinheim, 7th edn, 2010.
4 G. He, O. Shynkaruk, M. W. Lui and E. Rivard, *Chem. Rev.*, 2014, **114**, 7815.
5 S. Ishida, T. Iwamoto and M. Kira, *Organometallics*, 2010, **29**, 5526.
6 A. Rey Planells and A. Espinosa Ferao, *Inorg. Chem.*, 2022, **61**, 13846.
7 A. Espinosa Ferao and A. Rey Planells, *Chem. – Eur. J.*, 2023, **29**, e202302243.
8 A. Chiaroni, G. Hanquet, M. Lusinchi and C. Riche, *Acta Crystallogr., Sect. C: Cryst. Struct. Commun.*, 1995, **51**, 2047.
9 W. Sander, K. Schroeder, S. Muthusamy, A. Kirschfeld, W. Kappert, R. Boese, E. Kraka, C. Sosa and D. Cremer, *J. Am. Chem. Soc.*, 1997, **119**, 7265.
10 (*a*) P. R. Schreiner, H. P. Reisenauer, J. Romanski and G. Mloston, *J. Am. Chem. Soc.*, 2010, **132**, 7240; (*b*) H. P. Reisenauer, G. Mloston, J. Romanski and P. R. Schreiner, *Eur. J. Org. Chem.*, 2011, 6269; (*c*) T. Akasaka and W. Ando, *Phosphorus, Sulfur Silicon Relat. Elem.*, 1994, **95**, 437.
11 S. Bauer, A. Marinetti, L. Ricard and F. Mathey, *Angew. Chem., Int. Ed. Engl.*, 1990, **29**, 1166, (*Angew. Chem.*, 1990, **102**, 1188).
12 R. Streubel, A. Kusenberg, J. Jeske and P. G. Jones, *Angew. Chem., Int. Ed. Engl.*, 1995, **33**, 2427, (*Angew. Chem.*, 1994, **106**, 2564).
13 A. Özbolat, G. von Frantzius, J. M. Pérez, M. Nieger and R. Streubel, *Angew. Chem., Int. Ed.*, 2007, **46**, 9327, (*Angew. Chem.*, 2007, **119**, 9488).
14 (*a*) C. Albrecht, M. Bode, J. M. Pérez, J. Daniels, G. Schnakenburg and R. Streubel, *Dalton Trans.*, 2011, **40**, 2654; (*b*) V. Nesterov, G. Schnakenburg, A. Espinosa and R. Streubel, *Inorg. Chem.*, 2012, **51**, 12343; (*c*) J. Faßbender, N. Künemund, A. Espinosa Ferao, G. Schnakenburg and R. Streubel, *Organometallics*, 2018, **37**, 1331.
15 N. Volk, P. Malik, A. García Alcaraz, A. Espinosa Ferao and R. Streubel, *Coord. Chem. Rev.*, 2021, **437**, 213818.
16 F. Ramirez, A. S. Gulati and C. P. Smith, *J. Org. Chem.*, 1968, **33**, 13.
17 A. Espinosa Ferao, *Inorg. Chem.*, 2018, **57**, 8058.
18 G.-V. Röschenthaler, K. Sauerbrey and R. Schmutzler, *Eur. J. Inorg. Chem.*, 1978, **111**, 3105.
19 J. Faßbender, N. Volk, A. García Alcaraz, S. Balasubramaniam, A. Espinosa Ferao and R. Streubel, *Chem. Commun.*, 2023, **59**, 1285.
20 A. Espinosa Ferao and R. Streubel, *Eur. J. Inorg. Chem.*, 2017, 2707.
21 C. Murcia-García, A. Bauzá, G. Schnakenburg, A. Frontera and R. Streubel, *CrystEngComm*, 2015, **17**, 1769.
22 A. Schmer, P. Junker, A. Espinosa Ferao and R. Streubel, *Acc. Chem. Res.*, 2021, **54**, 1754.
23 C. Murcia García, PhD thesis, Rheinische Friedrich-Wilhelms-Universität Bonn, 2017.
24 A. Marinetti, F. Mathey, J. Fischer and A. Mitschler, *J. Chem. Soc., Chem. Commun.*, 1984, 45.
25 H. D. Flack and G. Bernardinelli, *Chirality*, 2008, **20**, 681.
26 (*a*) M. Schnebel, I. Weidner, R. Wartchow and H. Butenschön, *Eur. J. Org. Chem.*, 2003, **2003**, 4363; (*b*) J.-Y. Shie, J.-L. Zhu and Y.-P. Wu, *J. Chin. Chem. Soc.*, 2015, **62**, 665.
27 S. Sase, N. Kano and T. Kawashima, *J. Org. Chem.*, 2006, **71**, 5448.
28 V. Plack, J. R. Goerlich, H. Thönnessen, P. G. Jones and R. Schmutzler, *Heteroat. Chem.*, 1999, **10**, 277.
29 M. Nieger and M. W. M. Boras, CCDC 1843600:†Experimental Crystal Structure Determination, 2018.
30 S. Priya, M. S. Balakrishna, J. T. Mague and S. M. Mobin, *Inorg. Chem.*, 2003, **42**, 1272.
31 A. Espinosa Ferao, A. Rey Planells and R. Streubel, *Eur. J. Inorg. Chem.*, 2021, 348.
32 (*a*) M. Schröder, PhD thesis, Universität Kaiserslautern, 1999; (*b*) J. M. Perez, PhD thesis, Rheinische Friedrich-Wilhelms-Universität Bonn, 2010; (*c*) J. Marinas Pérez, C. Albrecht, H. Helten, G. Schnakenburg and R. Streubel, *Chem. Commun.*, 2010, **46**, 7244; (*d*) J. Marinas Pérez, H. Helten, B. Donnadieu, C. A. Reed and R. Streubel, *Angew. Chem., Int. Ed.*, 2010, **49**, 2615, (*Angew. Chem.*, 2010, **122**, 2670); (*e*) J. Faßbender, PhD thesis, 2017;

(*f*) J. Fassbender, G. Schnakenburg, D. P. Gates, A. Espinosa Ferao and R. Streubel, *Chem. Commun.*, 2018, **54**, 14013.

33 V. Plack, Diploma Thesis, Universität Braunschweig, 1993.

34 (*a*) V. Nesterov, R. Baierl, F. Hanusch, A. Espinosa Ferao and S. Inoue, *J. Am. Chem. Soc.*, 2019, **141**, 14576; (*b*) M. W. Stanford, J. I. Schweizer, M. Menche, G. S. Nichol, M. C. Holthausen and M. J. Cowley, *Angew. Chem., Int. Ed.*, 2019, **58**, 1329, (*Angew. Chem.*, 2019, **131**, 1343); (*c*) A. Espinosa Ferao, A. García Alcaraz, S. Zaragoza Noguera and R. Streubel, *Inorg. Chem.*, 2020, **59**, 12829.

35 D. Biskup, G. Schnakenburg, R. T. Boeré, A. Espinosa Ferao and R. Streubel, *Dalton Trans.*, 2023, **52**, 13781.